# Synergetic effects of $Cu_2O$ photocatalyst with titania and enhanced photoactivity under visible irradiation

**Dongfang Zhang**

*College of Science, Huazhong Agricultural University, Wuhan 430070, PR China*
*zdfbb@yahoo.cn*

**Abstract:** Heterogeneous $TiO_2/Cu_2O$ nanocomposite was synthesized for photocatalysis through surface impregnation in conjunction with the environmentally friendly soft chemical reduction strategy. The detailed structural, compositional, optical and photoelectrochemical properties of the obtained products are analyzed by X-ray diffraction (XRD), transmission electron microscopy (TEM), UV-Vis diffuse reflectance spectroscopy (UV-Vis DRS), photoluminescence spectra (PL) and electron spin resonance (ESR) spectroscopy techniques. Moreover, methyl orange (MO) dye was chosen as the probe molecule for evaluation of the photocatalytic activities of the samples under visible light ($\lambda > 420$ nm) irradiation. The experiments demonstrated that MO in aqueous solution was more efficiently photodegraded using $TiO_2/Cu_2O$ composite photocatalysts than pure $Cu_2O$ alone. This was attributed to the good crystallinity, wide visible-light absorption range, and the efficient electron-hole pair separation properties of the $TiO_2/Cu_2O$ nanoheterostructures. In this photocatalyst, visible-light-active $Cu_2O$ component was used as a medium to absorb photons and convert them into photogenerated charges, and $TiO_2$ nanoparticles were used as charge collectors to transport the photoinduced charges. The $TiO_2/Cu_2O$ hybrid material showed improved separation of photoinduced electron-hole pairs owing to the potential-energy differences between $Cu_2O$ and $TiO_2$, and therefore exhibited enhanced photocatalytic activity.

**Keywords:** photodecomposition, coupled semiconductor, methyl orange

## Introduction

Environmental pollution is currently one of the most important issues facing humanity. It has increased exponentially in the past few years and reached alarming properties in terms of its effects on living creatures. The civilian, commercial, and defense sectors of most advanced industrialized nations are faced with a tremendous set of environmental problems related to the remediation of hazardous wastes, contaminated groundwater, and the control of toxic air contaminants. Among them, dye pollutants have been a major source of environmental pollution because of their resistance to biodegradation [1]. Many conventional methods such as flocculation, reverse osmosis, and activated carbon absorption have been used to deal with wastewaters containing dyes [2]. Nonetheless, many shortcomings still exist in these methods because of the increasing number of refractory materials in wastewater effluents and difficulties in the totally removal of color and expensiveness. Up to now, studies show that heterogeneous photocatalytic oxidation technologies are promising methods [3–7] and a majority of research on photocatalytic oxidation technologies is focused on dye/$TiO_2$ system [8]. Titanium dioxide ($TiO_2$) is a promising catalyst in photodegradation of organic pollutants in water due to its inexpensiveness, strong oxidizing power, non-toxicity and long-term stability. However, photocatalytic efficiency of dye is limited because of slow interfacial electron transfer [9–11]. Therefore, it is urgent to develop highly efficient photocatalyst for dye decomposition under the illumination of visible light instead of UV light. There are several ways already been reported to improve the performance of catalysts, i. e., doping the catalyst to narrow the bandgap [12–15], nanostructing the catalyst [16–18] and mixing a narrow bandgap and a wide bandgap semiconductor together [19–21].

Recent study reveals that $Cu_2O$ powder could catalyze the decomposition of water into $H_2$ and $O_2$ under solar light, in which $Cu_2O$ exhibited good catalytic performance and stability [21]. Furthermore, nanosized $Cu_2O$ performs as an excellent visible-light-driven photocatalyst for the destruction of dye pollutants with a high degree of mineralization [22]. In this regard, sensitizing n-type $TiO_2$ with p-type active materials such as $Cu_2O$ is an efficient way to fabricate $TiO_2$-based catalysts with extended absorption in the visible and higher photocatalytic activity [23–27]. As is known, $Cu_2O$ is a p-type semiconductor with a narrow band gap ($E_0$= 1.9–2.2 eV). When a heterostructure forms between $TiO_2$ and $Cu_2O$, it can help to facilitate the separation and transportation of the photoinduced charge carriers in $TiO_2/Cu_2O$ composite, decrease the possibility of recombination and then enhance

the photocatalytic properties. Thus, the separation of photoinduced hole-electron ($h^+$-$e^-$) pairs can be accelerated by the potential difference at the p-n heterojunction interface. Moreover, the guest semiconductor with narrow band gap can facilitate the extended absorption in the visible. Concerning the high photocatalytic activity of nanosized $Cu_2O$, it is expected that the visible photoactivity of $Cu_2O$ for degradation of dye can be enhanced via synergetic effect of $TiO_2$ and $Cu_2O$ since the combination of visible-light photocatalyst $Cu_2O$ and n-type $TiO_2$ may be an ideal system to achieve an enhanced charge separation.

In this work, nano-scale $TiO_2/Cu_2O$ heterostructure composite was prepared through an alcohol-aqueous based chemical precipitation method. The structural, physicochemical properties and the photocatalytic characteristics of the as-prepared $TiO_2/Cu_2O$ hybrid materials were elucidated using a variety of techniques. Photocatalytic activities of the as-prepared nanocomposite catalysts were investigated in terms of the degradation action of methyl orange (MO) dye. The results show that the formation of a hetero-interface between $Cu_2O$ and $TiO_2$ facilitates the separation and transportation of the photoinduced charge carriers, depress the possibility of recombination and endow the catalyst with greatly enhanced photocatalytic activity. In addition to these aspects, photocatalytic process related to intermediates on catalyst surface was also studied and ·OH reactive species were found in aqueous $TiO_2/Cu_2O$ suspension under visible light irradiation. Therefore, a better understanding of the mechanism at molecular level may contribute to the design of more efficient photocatalysts.

## Materials and Methods

The reagents used in the experiments were copper sulfate (AR, Tianjin Chemical Company), PEG-400 (AR, Nanjing Chemical Company), tetrabutyl titanate (TBT, AR, Shanghai Chemical Company), hydrazine hydrate solution ($N_2H_4 \cdot H_2O$, CP, Tianjin Chemical Company) and 5,5-Dimethyl-1-pyrroline-N-oxide (DMPO) spin-trap reagent (Sigma Chemical Co.). Deionized and doubly distilled water was employed throughout this study. $TiO_2/Cu_2O$ composite oxides were prepared by the following method. In brief, 5.0 g of copper sulfate ($CuSO_4 \cdot 5H_2O$) was dissolved in 500 ml of distilled water, followed by the addition of 6.0 ml of PEG-400 under vigorous stirring. Afterward, 0.68 g of tetrabutyl titanate digested with 100 ml absolute ethanol was dropped into the solution of copper sulfate. A white precipitate was produced during the mixing. Then, 10 ml of 4 mol/L NaOH and 12 ml of 6 mol/L hydrazine hydrate solution ($N_2H_4 \cdot H_2O$) were dropped sequentially into the above slurry under vigorous stirring, and the resulting mixture was kept standing at temperature for 60 min. A yellow precipitate was then formed. It was filtered, washed with distilled water to neutral and further washed with acetone. The sample was then degassed at 400 °C in vacuum for 2 h. The as-prepared sample containing nominal molar ratio of 10 mol % $TiO_2$ was designated as $TiO_2/Cu_2O$ composite. For comparison, pure $TiO_2$ or $Cu_2O$ sample was also prepared through the above manner and were applied in the photocatalytic test to evaluate the effectiveness of decolorization of the dye solution.

X-ray powder diffraction (XRD) data were recorded at room temperature with an X-ray diffractometer (XRD-6000, Shimadzu Corporation) using Cu Kα irradiation (λ = 0.15406 nm), operated at 40 kV and 100 mA, which was used to identify the crystallographic information such as structure properties, chemical composition and phases of the products. The size and morphology of the acquired samples are characterized by transmission electron microscopic. The observations and recording of images were performed with a HITACHI H-7650 transmission electron microscope at 80 kV and a Gatan 832 CCD camera. UV-visible absorption spectra of the samples were recorded on a UV-vis spectrophotometer (Hitachi UV-3100) with an integrating sphere attachment. The analyzed range was 200—800 nm, and polytetrafluoroethylene was the reflectance standard. The photoluminescence (PL) emission spectra of the samples were measured with a RF-5301 PC spectrofluorophotometer (Shimadzu Corporation) by using the 320 nm line of a Xenon lamp as excitation source at room temperature. ESR signals of radicals spin-trapped by DMPO (5,5-Dimethyl-1-pyrroline-N-oxide) were recorded at ambient temperature on a Bruker ESP300E spectrometer (Bruker BioSpin, Germany). The irradiation source was a 300 W Xenon lamp equipped with a cutoff filter to remove the wavelength shorter than 400 nm. ESR signals were detected in the irradiated suspension of catalyst nanoparticles with organic nitrone compound (DMPO). Briefly, the spin traps were firstly premixed with the sample solution (catalyst-water suspension). After adding DMPO into the suspension, load the sample in a quartz capillary and transfer it into the ESR instrument to carry out the test. The typical instrumental settings were: center field: 3480.00 G, microwave frequency 9.77 GHz, microwave power 10.1 mW, sweep width 100 G, modulation frequency 100 kHz, modulation amplitude 0.5 G, receiver gain $2 \times 10^4$, time constant 81.92 ms, conversion time 40.96 ms and total scan time 41.9 s. The recorded

spectra were taken into a personal computer with an image scanner and converted to a g value scale referring to a $Mn^{2+}$ marker. The parameters observed here for DMPO—OH· are as follows, g is 2.00556, and $a_N = a_H$ is 14.95 G.

Photocatalytic efficiency of the obtained catalysts was estimated in terms of the degradation of methyl orange (MO) aqueous solution. The artificial light photocatalytic activity test is conducted in a quartz photoreactor with a cylindrical configuration. Photoirradiation was carried out by employing a 300-W Xenon lamp (a 420 nm cutoff filter was placed above the reactor to cutoff UV light) with emitted irradiation comparable to visible light. The distance between the surface of reaction solution and light source is adjusted to about 15 cm. A certain amount of photocatalyst powder (25 mg) is added to 150 ml aqueous methyl orange (10 mg/L) solution. Before switching on the activation light, the suspension is magnetically stirred in the dark for about 60 min to establish MO adsorption-desorption equilibrium as a reference point. The photocatalytic decomposition of MO aqueous solution was characterized by a UV-visible spectrometer based on the Beer-Lambert law. During the irradiation experiments, aliquots (5 ml) are withdrawn from the turbid solution at regular time intervals and are immediately centrifuged at 7000 rpm for 20 min to remove solids. The concentration of MO after illumination is monitored at $\lambda$ = 464 nm using UV-vis spectrophotometer (Spectrumlab 2450, Shimadzu Corporation). The degradation rate of the MO can be determined by the formula: $\eta\ \% = (B_0 - B_t)/B_0 \times 100\ \%$, where $B_0$, $B_t$ represents the initial absorbance and the absorbance of the aqueous MO after a certain period of illumination time t, respectively.

## Results and Discussion

The crystalline compositions and phase purity of the as-prepared samples were characterized by XRD patterns, as shown in Fig. 1. The XRD patterns show that pure titania consists of anatase phase, matching very well with the standard data. For the as-prepared $TiO_2$, diffractions that are attributable to anatase part of $TiO_2$ material are closely detectable at $2\psi$ = 25.3 ° (JCPDS 21-1272). For the as-prepared $Cu_2O$, the expected (110), (111), (200), (220), (311) and (222) diffraction peaks corresponding to crystal planes of the $Cu_2O$ crystals are presented, from which three characteristic peaks at $2\psi$ = 36.5 °, 42.4 °, 61.5 ° can be assigned to (111), (200) and (220) crystal planes of the single crystal $Cu_2O$ with cubic structure (JCPDS 05-667). The (111) reflection of the sample obtained is comparatively strong, which is probably due to the exposed orientation of the nanocrystalline $Cu_2O$. Besides, no other peaks due to Cu or CuO are observed, indicating the products are phase-pure $Cu_2O$ crystals, and there is no impurity such as cupric oxide or metallic copper. For $TiO_2/Cu_2O$ heterostructure, the XRD pattern shows that the as-prepared composite is the combination of $TiO_2$ and $Cu_2O$. However, the diffraction peaks belonging to $TiO_2$ were very weak and hardly to be observed for the sample 10 mol % $TiO_2/Cu_2O$, implying the low concentration of $TiO_2$ as well as the high dispersion of $TiO_2$ on $Cu_2O$. In addition, the average crystallite sizes of as-prepared $TiO_2/Cu_2O$ composite can be calculated by applying the Debye-Scherrer relation

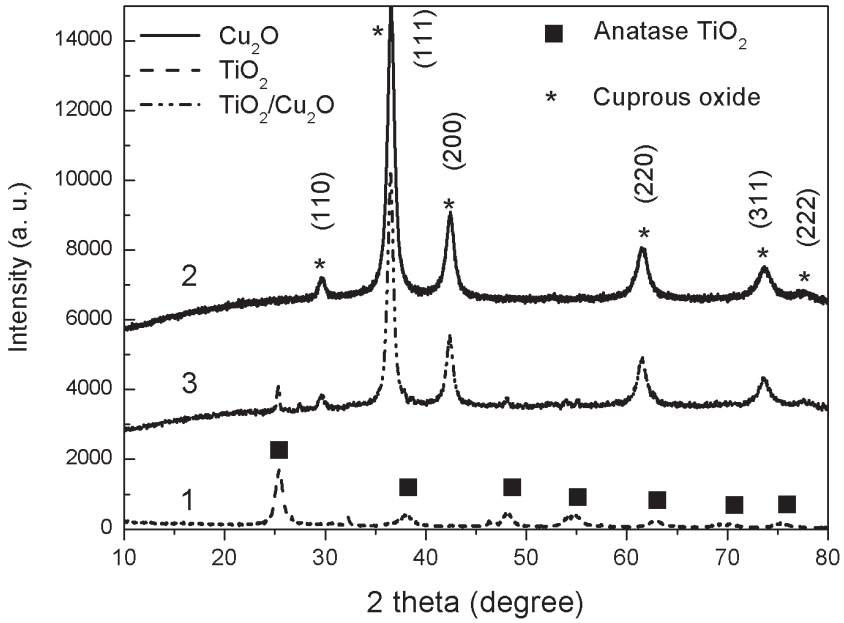


**Fig. 1.** X-ray diffraction patterns of (1) pure $TiO_2$ (2) pure $Cu_2O$ and (3) $TiO_2/Cu_2O$ nanocomposite.

on the cubic $Cu_2O$ (111) diffraction peak: $d = S \times \lambda / [w \times \cos(2\psi)]$, where d, S, λ, w, and ψ are the crystalline size in the direction vertical to the corresponding lattice plane, a shape constant of 0.89, wavelength of X-ray radiation (0.1541 nm), corrected full width at half maximum (FWHM) of the XRD peak, and angle of diffraction, respectively. The calculated average crystallite size from the above formula is about 25 nm. However, the employed Scherrer equation refers to the dimension of crystalline grain size that in general are different than the particles size that can be measured by imaging techniques. Moreover, the use of Scherrer equation for calculating particle sizes is only known to be about 10 % reliable. Therefore, TEM images could help solve the problem by giving a clear picture of the morphology and right sizes for small particles. The TEM image at a specific magnification of the as-prepared $TiO_2/Cu_2O$ composite is shown in Fig. 2. The result confirms the nanoparticulate nature of the composite, which contains different size particles with irregular round shape. The size of the observed $TiO_2/Cu_2O$ composite particles estimated from the TEM graph was normally about 20—40 nm, which agrees with that obtained from XRD analysis. Generally, it can be said that the small particle size is expected to reduce the recombination opportunities of the photogenerated electron-hole ($e^-$-$h^+$) pairs in the volume, which can effectively move to the surface to participate the redox reaction. Furthermore, smaller particles have a larger surface area and thus provide more available surface active sites for the reaction, which is vital to for the good photoactivities of semiconductor photocatalysts.

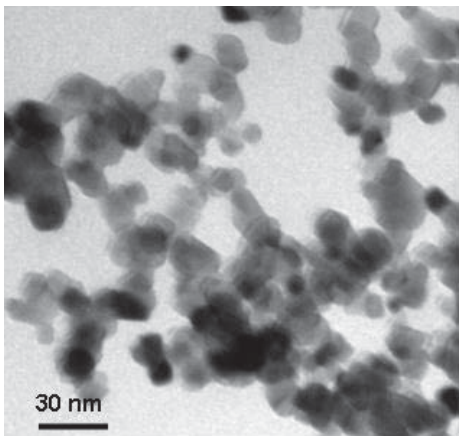


**Fig. 2.** A representative TEM micrograph of the as-prepared $TiO_2/Cu_2O$ nanocomposite.

The optical absorption property is a key factor controlling the photocatalytic activity of a catalyst. In order to explore the optical response of the obtained $TiO_2/Cu_2O$ nanocomposite, pure $TiO_2$ and $Cu_2O$ nanoparticles, the UV-vis reflectance analysis has been performed on the powder samples, as is shown in Fig. 3. The diffuse reflectance measurements were converted into the equivalent absorption coefficient using the Kubelka-Munk method, as depicted by $\alpha = (1 - R)^2/2R = F(R)$ [28—30], where α is the optical absorption coefficient, R is the reflectance of the semiconductor, $R = 10^{-A}$, and A is the optical absorbance, and F(R) is the Kubelka-Munk function. From the graph, it is found that the as-prepared $TiO_2/Cu_2O$ and pure $Cu_2O$ samples do not display distinct absorption edge and the absorption curves of which exhibit a clear

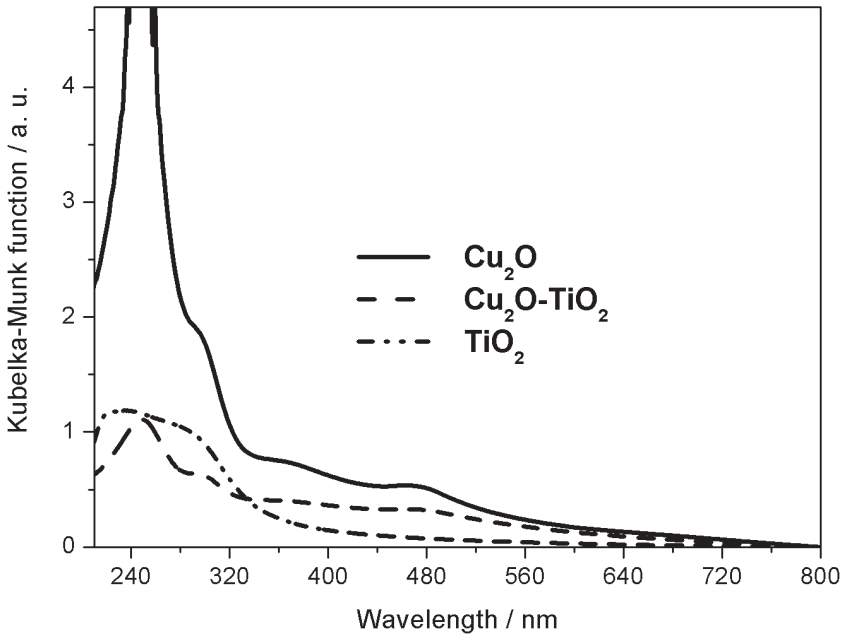


**Fig. 3.** UV-Vis diffuse reflectance spectra of pure $Cu_2O$, $TiO_2$ and $TiO_2/Cu_2O$ nanocomposite.

absorption within the whole visible region, which suggest that the ability for visible light absorption is improved to a certain degree. The result indicates that $TiO_2/Cu_2O$ is potentially good photocatalyst for sunlight-driven application and the enhanced light-absorption capability is favourable for photocatalytic activity. By comparison, pure $TiO_2$ sample mainly absorbed ultraviolet radiation of less than 400 nm and has no obvious absorption in the visible region (> 420 nm), and the absorption edge of pure $TiO_2$ is about 380 nm, which is associated with the intrinsic band gap absorption of $TiO_2$ corresponding to $O_{2p} \rightarrow Ti_{3d}$ charge transfer. In this context, the as-prepared $TiO_2/Cu_2O$ composite exhibited not only strong absorption in the ultraviolet region but also adequate absorption in the visible region in facilitating the photodegradation efficiency. The aforementioned result confirms that $TiO_2/Cu_2O$ heterogeneous structure greatly ameliorated the light absorption properties of the $TiO_2/Cu_2O$ composite and could absorb more photons, thus enhancing light-harvesting and increasing the quantity of photogenerated electrons and holes. As a result, $TiO_2/Cu_2O$ composite exhibit a higher absorbance between 400 and 700 nm than that of pure $TiO_2$, which makes the as-prepared $TiO_2/Cu_2O$ can be used under visible light. Overall, the $TiO_2/Cu_2O$ composites absorb significant amounts of visible light, indicating an enhanced ability to respond towards visible range. The large red shift in optical response can be attributed to several factors. The first comes from the integration effect of the band gap of the composite semiconductor. When $TiO_2$ with a relative wide band gap combines with a narrow band gap $Cu_2O$, the band gap of the composite $TiO_2/Cu_2O$ will be further narrowed. The second factor is due to the interface effect that potentials of band edges are influenced by each other in the studied composite [31]. The extended absorbance of $TiO_2/Cu_2O$ composite photocatalysts in the visible range is thus of practical importance, because efficient utilization of sunlight or solar spectrum for the photocatalytic degradation reaction could be achieved and it can explain at all why the composite should be active upon visible light excitation and the described flow of electrons and holes.

Photoluminescence (PL) is the spontaneous emission of light from a material under optical excitation. The exciton emission and defect emission from discrete electronic states can be observed from the PL spectrum even though reactive and emitting states may be different. Features of the emission spectrum can be used to identify surface, interface, and impurity levels and a correlation of fluorescence intensities with activities is reliable [32]. The intensity of the PL signal provides information on the relative rates of charge carrier trapping, migration and transfer, and benefit for understanding the fate of electron-hole pairs in semiconductor particles [33–35]. Generally, a decrease in the PL intensity indicates a decrease in the recombination rate and, thus, an enhanced charge separation efficiency of photoinduced electrons and holes [36]. Fig. 4 shows the room temperature PL spectra of the $TiO_2/Cu_2O$ composite, pure $TiO_2$ and $Cu_2O$ samples with the excitation wavelength at 320 nm. We can observe that both samples show a strong broad emission

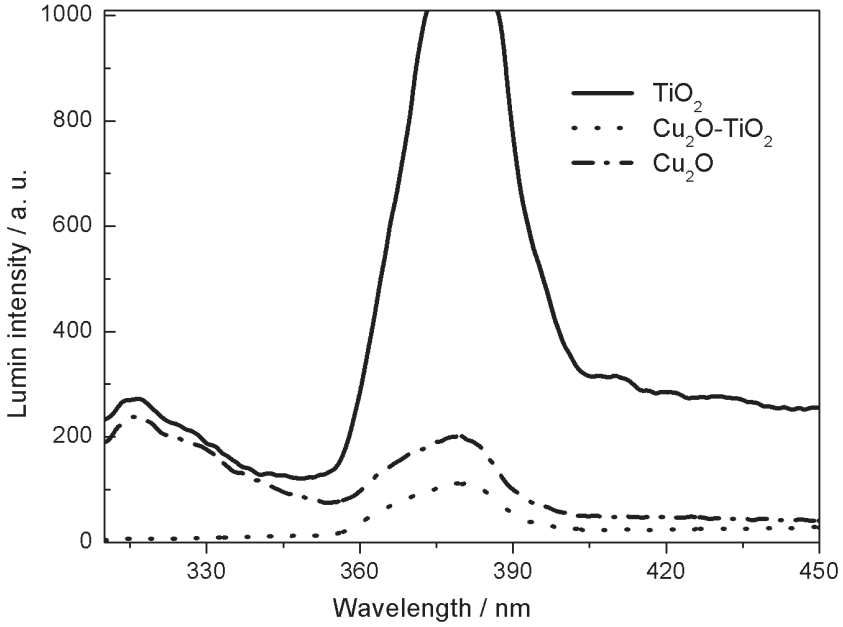


**Fig. 4.** Emission PL spectra ($\lambda_{ex}$ = 320 nm) of pure $Cu_2O$, $TiO_2$ and $TiO_2/Cu_2O$ nanocomposite.

peak around 380 nm. These PL signals can be attributed to the band-band PL phenomenon. Usually, the band-band PL spectrum associates with the separation situation of photo-generated charge carriers. In the given PL spectra, the bands in the visible region appeared in the case of $TiO_2$ drops after impregnating with $Cu_2O$. Thus it can be speculated that surface states/oxygen vacancies responsible for surface recombination is effectively suppressed for the composite. In addition, the pristine peak drastically reduces in its intensity for the composite. It possibly because the different redox energy levels of conduction and valence bands for $Cu_2O$ and $TiO_2$ led to the interfacial charge transfer to impair the recombination of electron-hole pairs in $TiO_2/Cu_2O$ composite and this heterogeneous structure can effective diminish the $e^-/h^+$ recombination. The slower recombination rate will favor to the photocatalytic reaction and retain the stability of quantum efficiency throughout the reaction process. This result suggests that both bulk and surface recombination of charge carriers are effectively suppressed in the composite. Therefore, coupling $Cu_2O$ with $TiO_2$ is helpful to suppress the recombination of charge carriers and consequently leading to enhanced photocatalytic oxidation activity.

DMPO traps hydroxyl and superoxide radicals with the formation of nitrone spin adducts which are rather stable and can be detected by ESR spectroscopy [37]. The ESR spin-trap technique (with DMPO) was employed to probe the nature of the reactive oxygen species generated from the as-prepared pure $Cu_2O$, $TiO_2$ and $TiO_2/Cu_2O$ nanocomposite. Fig. 5 illustrates the electron paramagnetic resonance spectra of the corresponding systems in aqueous solution under visible-light illumination for 30 min. It was found that the intensity of the peaks further increased with the increase of irradiation time and basically reached stable state in 15 min, therefore the intensity of the DMPO—·OH adduct peak produced in 30 min irradiation was nearly similar to that in 15 min irradiation. Moreover, almost no ESR signals were observed when the reaction was performed in the dark in the presence of catalyst/DMPO suspension or when DMPO alone was present. This means that irradiation is essential for the generation of ·OH on the surface of the catalyst. There are the characteristic four peaks of DMPO—·OH with intensity 1:2:2:1 in the ESR signal [38]. Furthermore, the peak intensity of ·OH generated from $TiO_2/Cu_2O$ was greatly higher than that from pure $Cu_2O$ or pure $TiO_2$, which indicated the visible-light-driven photocatalytic activity of $TiO_2/Cu_2O$ is the best among all samples. Since many more ·OH radicals were produced with $TiO_2/Cu_2O$ composite than parent $Cu_2O$ or $TiO_2$, implying that a small quantity of $TiO_2$ combining with $Cu_2O$ can accelerate the separation of photo-induced electrons and holes on $Cu_2O$ as well as promote the decomposition of water to generate ·OH. The evidence that ·OH was produced on the surface of visible illuminated $TiO_2/Cu_2O$ provides a solid indication that the catalyst can be efficiently excited by visible light to create electron-hole pairs

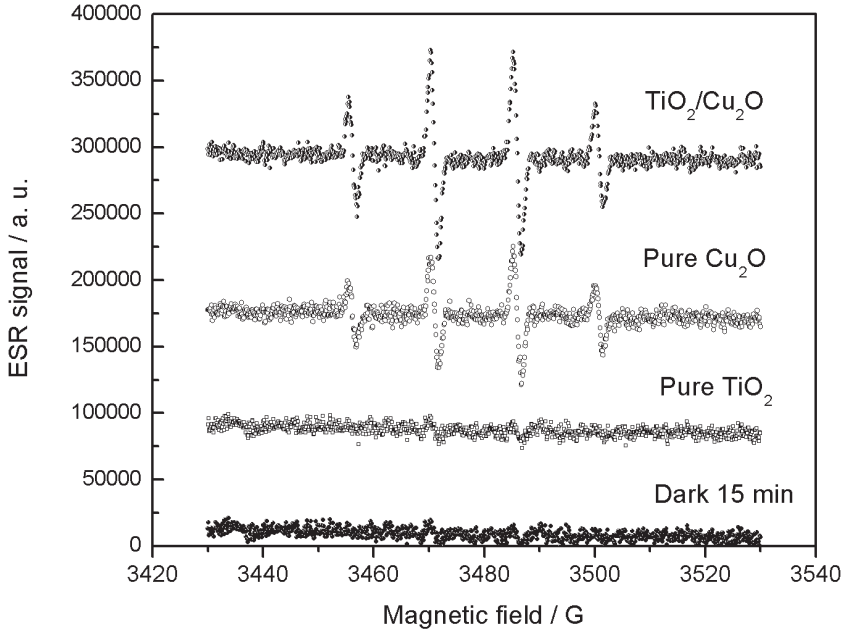


**Fig. 5.** DMPO spin-trapping ESR spectra under visible irradiation in the as-synthesized pure $Cu_2O$, $TiO_2$ and $TiO_2/Cu_2O$ nanocomposite.

and that the charge separation is maintained long enough to react with adsorbed oxygen/$H_2O$ and to produce a series of active oxygen radicals which finally decompose organic compounds. The ESR signals for the spin adducts DMPOOOH· and/or DMPO-$O_2\cdot^-$ may possibly involved. However, these latter two spin adducts were not observed in this study. It is known that the superoxide radical anions are produced first and remain stable in an organic solvent medium (at least in methanol), while the superoxide radical anions are unstable in $H_2O$ system, for example, $O_2\cdot^-$ readily converted to $H_2O_2$ and $O_2$ [39]. Another possible reason is the slow reactions between ·OOH/$O_2\cdot^-$ and DMPO, which are several orders of magnitude lower than formation of the DMPO—·OH spin adduct since the $O_2\cdot^-$ radicals in water are short-lived transient and undergo facile disproportionation rather than slow reaction with DMPO [40]. Besides that, the transition from DMPO—OOH· and DMPO-$O_2\cdot^-$ to DMPO—·OH was estimated to be too fast to be detected. Concluding, neither ·OH nor $O_2\cdot^-$ was formed in the visible light illuminated $TiO_2$ suspension, indicating no reactive oxygen species generated on neat $TiO_2$.

In the present case, methyl orange (MO) dye was employed as a target pollutant to evaluate the real performance of the as-prepared catalyst since the oxide of MO is the major light absorbing species without sensitization under visible-light illumination such as Rhodamine-B [41]. The optical behavior of MO in solution was analyzed by measuring its maximal absorbance at 464 nm. The preliminary test demonstrates that no dye degradation in solution can be observed in the absence of the photocatalyst at the same conditions from a blank experiment. However, under visible light ($\lambda$ > 420 nm) illumination, $TiO_2$ can not be activated due to its large band gap ($E_0$ = 3.2 eV). Therefore, we can only note a continual fading of the coloration of MO solution as a function of reaction time in the presence of the $Cu_2O$ or $TiO_2$/$Cu_2O$ samples, implying a steady and continuous degradation of the organic dye since only $Cu_2O$ is the main active species that can be excited under visible light. Fig. 6A shows that $TiO_2$/$Cu_2O$ composite exhibits the highest photocatalytic activity for decomposing MO. At the same time, Fig. 6B reveals a gradual decrease of MO aqueous absorption at the wavelength of 464 nm under visible light. The present experiment demonstrates that the colors of the supernatant of MO solution changes from yellow to colorless observed by the naked eye after visible light irradiation for 60 min. The reason for this phenomenon is that about 90 % of MO is decolorized, showing the excellent photocatalytic activity of the as-prepared sample under visible light irradiation.

The above results indicate that the $TiO_2$/$Cu_2O$ composite have much higher photocatalytic activity than pure $Cu_2O$. The enhanced activity is probably attributed to the improved optical absorption and the heterostructure which favors the separation of photo-introduced electrons/holes pairs in $TiO_2$/$Cu_2O$ heterostructures. According to the flat band potentials of the valence and conduction bands (versus the normal hydrogen electrode (NHE)) for $TiO_2$ and $Cu_2O$ with their band energy [3], the conduction band (CB) level of $Cu_2O$ lies at –1.52 eV, which is more negative than the conduction band level of $TiO_2$ (–0.23 eV, NHE). In other words, the CB level of $Cu_2O$ is situated above the CB level of $TiO_2$. In this case, thermodynamic conditions favor the electron transfer from $Cu_2O$ to $TiO_2$. Under visible light irradiation, $Cu_2O$ can be activated according to process: $Cu_2O + h\nu \rightarrow Cu_2O(e^-) + Cu_2O(h^+)$, the generated electrons in $Cu_2O$ are then slip to the conduction band (CB) of $TiO_2$. This transfer process is thermodynamically favorable due to the known fact that CB of $Cu_2O$ lies above that of $TiO_2$. Meanwhile, the generated electrons probably react with dissolved oxygen molecules to produce superoxide radical anions ($O_2\bullet^-$) via processes: $TiO_2(e^-) + O_2 \rightarrow TiO_2 + O_2\cdot^-$ or $Cu_2O(e^-) + O_2 \rightarrow Cu_2O + O_2\cdot^-$ to decompose organic pollutant via process: Dye + $O_2\cdot^- \rightarrow$ Photobleached products, while the holes of $Cu_2O$ may react with some $OH^-$ or $H_2O$ to produce active hydroxyl radicals (OH·) via process: $Cu_2O(h^+) + OH^- \rightarrow Cu_2O + OH\cdot$ to decompose organic pollutant (Dye + OH· → Photobleached products). These radicals are the main oxidizing agents promoting MO decomposition. As evidence of the presence of the radical species during the photocatalysis course, it could be inferred that MO was degraded mainly by means of OH·. According to our previous discussion, we think that coupling of $Cu_2O$ and $TiO_2$ extends the absorption range to visible light region and promotes electron-hole pair separation. The energetically excited species are active and capable of initiating many chemical reactions, usually by the production of radical species at the semiconductors surface. However, the recombination of the photogenerated electrons and holes occurs very quickly. The photocatalytic efficiency depends on the competition between the surface charge carrier transfer rate and the electron-hole recombination rate [42]. If the recombination occurs too fast, there is no time for any other chemical reaction to occur. While the $Cu_2O$ coupled $TiO_2$ photocatalyst was irradiated, the electrons were excited from the valance band to the conduction band and then the photoinduced

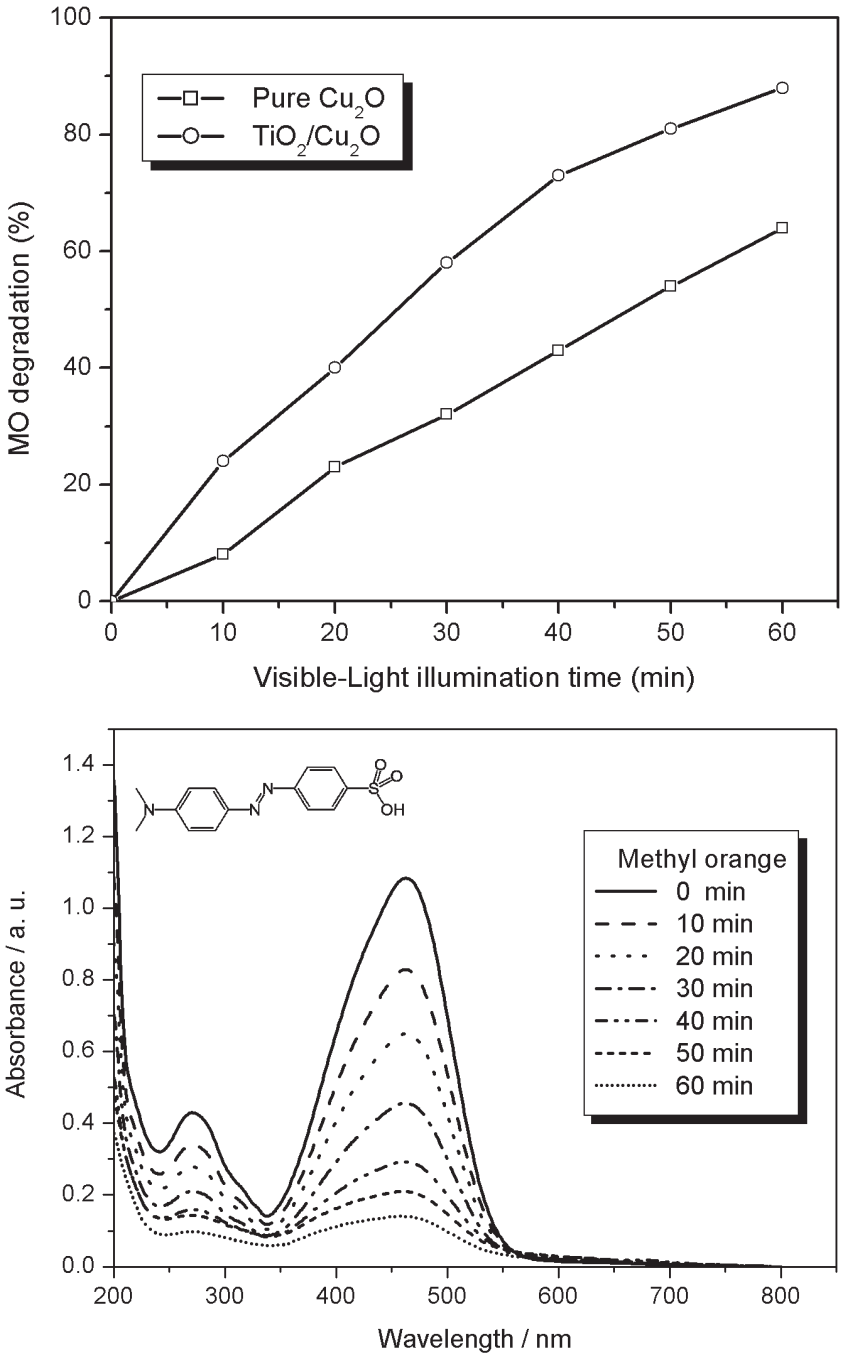


**Fig. 6.** Relative concentration variation of MO solution (10 mg/L) with irradiation time (A — on top). Temporal evolution of the absorption spectra of the treated MO over $TiO_2/Cu_2O$ composite catalyst (B — bottom).

electron-hole pairs could be effectively separated at the interface of the two semiconductors based on our PL data. Therefore, pure $Cu_2O$ has lower photocatalytic activity under visible light compared with the $TiO_2/Cu_2O$ heterostructure due to the transient recombination of photo-induced electrons and holes. Conversely, the effective formation of heterojunctions affects the charge separation properties of the composite photocatalyst, that is, the electrons generated on $Cu_2O$ by visible irradiation were automatically drifted to the CB of $TiO_2$ so that the recombination of electron-hole (e-h) pairs was suppressed and thus the quantum efficiency was enhanced. As a result, a higher photocatalytic oxidation activity is achieved for the $TiO_2/Cu_2O$ composite.

## Conclusions

In summary, $TiO_2/Cu_2O$ binary hybrid catalyst was synthesized via soft chemical reduction process. The experimental results revealed that the $TiO_2$/

$Cu_2O$ composite exhibits superior visible-light photocatalysis compared with their $TiO_2$ or $Cu_2O$ component in the photodecomposition of aqueous MO dye. The synergistic effect of bicomponent shows that the formation of hetero-junction generates a built-in potential gradient. This induces a more efficient separation of excess charge carriers and retards the recombination of charge pairs, thereby facilitating the interparticle electron transfer at the $TiO_2/Cu_2O$ interfaces and makes the composite system disappear dye more rapidly than only $TiO_2$ or $Cu_2O$. The present study demonstrates that hybridizing semiconductor nanoparticles with different band gaps and band positions should serve as a model for the development of semiconductor hybrids with multiple components. Moreover, this work provides a method to exploit highly efficient photocatalyst that can work under solar light irradiation as well as for promising applications in photocatalysis fields for the treatment of organic-polluted water.

***Acknowledgments***

*This work was supported by the Natural Science Foundation of Hubei Province of China (2011CDB148).*

## References

1. Zhang Y, Li DL, Chen Y, Wang XH, Wang ST (2009) Appl Catal B 86: 182–189.
2. Herrera F, Lopez A, Mascolo G, Albers P, Kiwi J (2001) Water Res 35: 750–760.
3. Linsebigler AL, Lu G, Yates JT (1995) Chem Rev 95: 735–758.
4. Saravanan R, Karthikeyan N, Gupta VK, Thirumal E, Thangadurai P, Narayanan V, Stephen A (2013) Mater Sci Eng C 33: 2235–2244.
5. Zhang JW, Zhang M, Jin ZS, Wang JJ, Zhang ZJ (2012) Appl Surf Sci 258: 3991–3999.
6. Zhang SW, Li JX, Niu HH, Xu WQ, Xu JZ, Hu WP, Wang XK (2013) ChemPlusChem 78: 192–199.
7. Zhang K, Jing DW, Chen QY, Guo LJ (2010) Int J Hydrogen Energy 35: 2048–2057.
8. Hanaor DAH, Sorrell CC (2011) J Mater Sci 46: 855–874.
9. Zhang H, Lv XJ, Li YM, Wang Y, Li JH (2010) ACS Nano 4: 380–386.
10. Zhang YH, Tang ZR, Fu XZ, Xu YJ (2010) ACS Nano 4: 7303–7314.
11. Zhang YH, Tang ZR, Fu XZ, Xu YJ (2011) ACS Nano 5: 7426–7435.
12. Zhang SM, Chen YY, Yu Y, Wu HH, Wang SR, Zhu BL, Huang WP, Wu SH (2008) J Nanopart Res 10: 871–875.
13. Zhang XT, Zhou GW, Zhang HY, Wu CC, Song HB (2011) Transition Met Chem 36: 217–222.
14. Zhang JZ, Chen XG, Shen YD, Li YW, Hu ZG, Chu JH (2011) Phys. Chem. Chem. Phys 13: 13096–13105.
15. Wu YM, Xing MY, Zhang JL (2011) J Hazard Mater 192: 368–373.
16. Zhang ZJ, Wang WZ, Wang L, Sun SM (2012) ACS Appl Mater Interfaces 4: 593–597.
17. Zhang J, Li LP, Yan TJ, Li GS (2011) J Phys Chem C 115: 13820–13828.
18. Zhang YH, Tang ZR, Fu XZ, Xu YJ (2011) Appl Catal B 106: 445–452.
19. Saravanan R, Shankar H, Prakash T, Narayanan V, Stephen A (2011) Mater Chem Phys 125: 277–280.
20. Zhang X, Zhang LZ, Xie TF, Wang DJ (2009) J Phys Chem C 113: 7371–7378.
21. Hara M, Kondo T, Komoda M, Ikeda S, Shinohara K, Tanaka A, Kondo JN, Domen K (1998) Chem Commun 3: 357–358.
22. Ma L, Li J, Sun H, Qiu M, Wang J, Chen J, Yu Y (2010) Mater Res Bull 45: 961–968.
23. Zhang SS, Zhang SQ, Peng F, Zhang HM, Liu HW, Zhao HJ (2011) Electrochem Commun 13: 861–864.
24. Han CH, Li ZY, Shen JY (2009) J Hazard Mater 168: 215–219.
25. Wang XF, Chen GM, Zhang J (2013) Catal Commun 31: 57–61.
26. Xiu FR, Zhang FS (2009) J Hazard Mater 172: 1458–1463
27. Li LK, Xu LL, Shi WD, Guan JG (2013) Int J Hydrogen Energ 38: 816–822.
28. Riaz N, Chong FK, Dutta BK, Man ZB, Khan MS, Nurlaela E (2012) Chem Eng J 185–186: 108–119.
29. Sathishkumar P, Sweena R, Wu JJ, Anandan S (2011) Chem Eng J 171: 136–140.
30. Anandan S, Lee GJ, Chen PK, Fan CH, Wu JJ (2010) Ind Eng Chem Res 49: 9729–9737.
31. Sathishkumar P, Mangalaraja RV, Anandan S, Ashokkumar M (2013) Chem Eng J 220: 302–310.
32. Zhang YP, Pan CX (2011) J Mater Sci 46: 2622–2626.
33. Karunakaran C, Abiramasundari G, Gomathisankar P, Manikandan G, Anandi V (2011) Mater Res Bull 46: 1586–1592.
34. Duan F, Zheng Y, Chen MQ (2011) Appl Surf Sci 257: 1972–1978.
35. Wang JX, Ruan H, Li WJ, Li DZ, Hu Y, Chen J, Shao Y, Zheng Y (2012) J Phys Chem C 116: 13935–13943.
36. Wang D, Xue G, Zhen Y, Fu F, Li D (2012) J Mater Chem 22: 4751–4758.
37. Wang Z, Ma W, Chen C, Ji W, Zhao J (2011) Chem Eng J 170, 353–362.
38. Yan GL, Chen J, Hua ZZ (2009) J Photoch Photobio A 207: 153–159.
39. Zhang JW, Jin ZS, Feng CX, Yu LG, Zhang JW, Zhang ZJ (2011) J Solid State Chem 184: 3066–3073.
40. Coronado JM, Soria J (2007) Catal Today 123: 37–41.
41. Wang F, Zhang K (2011) J Mol Catal A 345: 101–107.
42. Zhang GY, Sun YQ, Gao DZ, Xu YY (2010) Mater Res Bull 45: 755–760.